applied sciences

MDPI

*Article*

# Evolution Laws of Water-Flowing Fracture Zone and Mine Pressure in Mining Shallow-Buried, Hard, and Extra-Thick Coal Seams

**Zhongya Wu [1,2], Qiang Sun [1,2,*] and Yunbo Wang [1,2]**

[1] School of Mines, China University of Mining and Technology, Xuzhou 221116, China; zhongyawu@126.com (Z.W.)
[2] State Key Laboratory for Fine Exploration and Intelligent Development of Coal Resources, China University of Mining and Technology, Xuzhou 221116, China
* Correspondence: kkysun@126.com

**Abstract:** Shallow-buried, hard, and extra-thick coal seams are very common in Xinjiang, China, but there are relatively few studies on the mine pressure law and the development characteristics of water-flowing fracture zones (WFFZs) during the mining of such coal seams. In this paper, the mine pressure of the top coal caving face in a shallow, hard coal seam with a hard roof and full bedrock (SHCSHRFB) is analysed, the laws of the surrounding rock deformation and stress of the open-off cut and roadway in the large-mining-height top coal caving face are studied, the characteristics of roof-breaking and overburden fracture development are analysed using the physical similarity simulation method, supporting suggestions for roadways are put forward, and three development stages of the WFFZ are analysed. Field monitoring shows that the hydraulic support stress in SHCSHRFB is weak, but the coal wall and roadway stability are good, which is significantly different from the results in the typical shallow-buried thin bedrock working faces. The measured height of the WFFZ is close to the physical similarity simulation results, but quite different from those arising from use of the empirical formula.

**Keywords:** shallow coal seam; hard coal and roof; mine pressure; water-flowing fracture zone; physical similarity simulation



**Citation:** Wu, Z.; Sun, Q.; Wang, Y. Evolution Laws of Water-Flowing Fracture Zone and Mine Pressure in Mining Shallow-Buried, Hard, and Extra-Thick Coal Seams. *Appl. Sci.* **2024**, *14*, 2915. https://doi.org/10.3390/app14072915

Academic Editors: Zhongliang Wang and Markos Tranos

Received: 26 December 2023
Revised: 11 March 2024
Accepted: 13 March 2024
Published: 29 March 2024



## 1. Introduction

The coal resources detected in Xinjiang mines amount to about 2.2 trillion tons, accounting for about 40% of the total coal resources in China, and the coal development potential is huge [1]. The coal seams in the Xinjiang region are generally buried at a shallow depth and are thick; such geological conditions, involving hard coal seam and a hard roof, exist in many of the mines, providing significantly different conditions from those in the mines in central or eastern China [2]. With the special geological conditions pertaining to coal seams in Xinjiang and the existence of many new mines with insufficient mining experience, it is important to study the rock pressures, roof-breaking, and the development of WFFZ in the mining of SHCSHRFB.

The burial depth of such coal seams does not exceed 150 m. Typical shallow buried coal seams usually have thick topsoil and thin bedrock; the thickness ratio of bedrock to topsoil (TRBT) is generally less than 1. Its overlying stratum is usually a single main key stratum structure; breaks in the working face roof often occur in the form of an overall cut-down, leading to stepped subsidence, and the workface is subject to dynamic load [3–5]. Many scholars have investigated the rock pressure, overlying strata movement, and breaking behaviour for shallow-buried coal seams. Gu Minshuai, Du Feng, et al. [6–8] assessed the effects of mining area topography on shallow coal seam working face rock pressure and proposed a rock pressure prediction method and hydraulic support working resistance

design process, forming technical measures to reduce the possibility of rock pressure disasters occurring in shallow working faces by adjusting the layout and the advance speed of the working face. Debjeet Mondal studied the strata behaviour in the destressed zone of a shallow Indian longwall panel with a hard sandstone cover, finding that the overlying strata behave violently and microseismic events are intense [9].

Many scholars have investigated the overlying stratal movement and rock pressure on hard roof working faces, analysing the structure, the breaking pattern of the hard strata and the rock pressure [10,11], the coupling relationship between the support and the surrounding rock, and the effects of the strong rock pressure on the working face, and a mining height optimisation design method has been proposed [12–14]. Roof pressure weakening methods, such as hydraulic fracturing, blasting pre-cracking and supercritical $CO_2$ fracturing, and coal face undercutting, have been applied or studied [15–18]. In terms of research on overburden failure or WFFZ, empirical formulae, indoor tests, mechanical and simulation methods, and field monitoring methods are mainly used for research [19,20]. The empirical formula generally induces significant errors when predicting the development height of the water-conducting fracture zone with special overlying rock structure and mining technology, and the physical similarity simulation and numerical simulation methods usually need to be verified by in situ measurements due to the model simplifications and assumptions made regarding the characteristics of the geological conditions [21–23]. Some scholars proposed new research methods for the development of WFFZ; for example, optical fibre technology is used for monitoring, a more accurate conceptual model of fracture zone is proposed, and new predictive analysis methods, such as the neural network method, are adopted [24–26]. Researchers analysed the relationship between the development of the WFFZ and factors such as the advance speed, mining range, and mining height; water-preserving mining technology was created to control the development height of WFFZ by backfilling the goaf, limiting the mining thickness, using narrow strip mining, and other methods [27–29].

In general, research into hard-roofed or shallow coal seams in China is mainly concentrated in the Shendong or Datong mining areas, and is mostly conducted on shallow coal seams with a TRBT of less than 1. There are few studies on stratal movement, rock pressure characteristics, and the development of WFFZs with SHCSHRFB. Using the engineering background of Yushuling Coal Mine in Kuqa County, Xinjiang, we conducted a study of the rock pressure and strata breaking of a top coal caving face in an SHCSHRFB. The engineering and geological conditions were first introduced; then, the changes in the abutment pressure, and the stress and deformation characteristics of the roadway during the advance of the working face, were assessed via numerical simulation. The roof-breaking characteristics, the WFFZ, and the front abutment pressure were studied through physical similarity simulation. Finally, the hydraulic support pressure, roadway deformation, and height of the WFFZ were measured in situ. The research results can provide technical guidance for the safe and efficient mining of SBDHETCS in Xinjiang.

## 2. Overview of the Study Area

### *2.1. Geological Condition*

Yushuling Coal Mine is located in the northern part of Kuqa County, Aksu Prefecture, Xinjiang. It is the junction area between the southern foot of the Tianshan Mountains and the northern edge of the Tarim Basin. Yushuling Coal Mine uses inclined shaft development, with a production capacity of 1.2 million tons per year. There are five mineable coal seams in the minefield area, namely the No. 5, No. 7, No. 8, No. 10, and No. 12 coal seams. The coal seams of the Yushuling Coal Mine are generally monoclinic in shape, with a high northwest and low southeast, and the mine surface altitude range is between 1743.80 m and 1907.77 m.

The 110501 working face is the first mining working face of the mine, which uses top coal caving technology. The average coal seam inclination and thickness are 10° and 8.6 m, respectively; the 110501 working face was designed with a shear mining height of

4.0 m and a caving height of 4.6 m. Due to the large amount of water accumulated in the overlying rock at the north-west corner of the 110501 working face, to ensure safe mining, the working face was arranged in a knife-handle style. The initial cut-off length of the working face is 102 m, and it is lengthened to 155 m after bypassing the water accumulation area. The 110501 working face has a burial depth of 100 m to 150 m, and the overlying rock is full bedrock without topsoil. The location and layout of the Yushuling Coal Mine in China is shown in Figure 1.

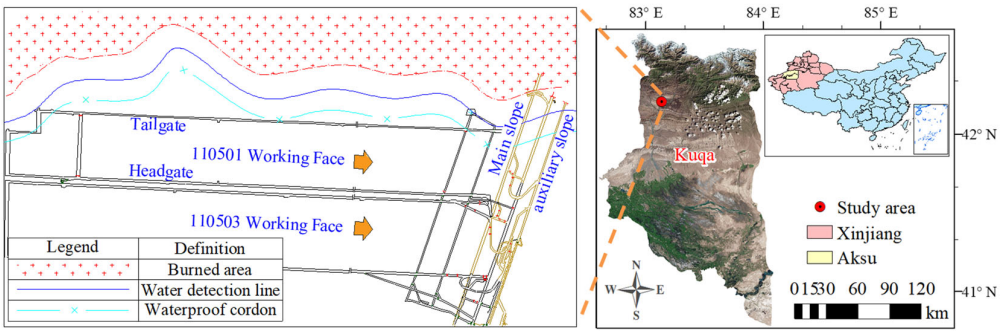


**Figure 1.** Location and layout of the Yushuling Coal Mine.

The UCS, tensile strength, and cohesion of the No. 5 coal seam are 23.06 MPa, 0.78 MPa, and 11.17 MPa, respectively, the internal friction angle is 48.23°, the Protodyakonov coefficient is 3.8, and the coal seam is hard and complete. The 110501 working face has no false roof; the immediate roof is mainly siltstone, containing fine sandstone and coarse sandstone, with an RQD of 0.47 and a thickness of between 0 and 4.83 m. The main roof is mainly grey-white siltstone, containing fine sandstone, medium sandstone and coarse gravel sandstone, with an RQD of 0.68 and a thickness of between 8 and 14 m. The UCS values of the immediate roof and the main roof of the working face are 25.06 MPa and 46.35 MPa, respectively, and the main roof is hard, with a Protodyakonov coefficient of 7.5. The borehole diagram of the Yushuling Coal Mine is shown in Figure 2.

| Lithology | Thickness / m | Depth / m | Columnar | Description | Strata type |
|---|---|---|---|---|---|
| Gritstone | 34.08 | 34.08 | | Containing feldspar, quartz, and gravel, intact, columnar | Top bedrock Hark |
| Glutenite | 1.80 | 35.88 | | Mainly metamorphic and sedimentary rock, columnar | |
| Packsand | 7.40 | 43.28 | | Containing feldspar, quartz, calcareous cement | |
| Gritstone | 11.68 | 54.96 | | Containing quartz, calcareous cement, columnar | Hard |
| Glutenite | 1.70 | 56.66 | | Mainly metamorphic and sedimentary rocks | |
| Coal | 0.60 | 57.26 | | Lumpy, mainly containing dark coal | |
| Packsand | 13.22 | 70.48 | | Containing feldspar, quartz, calcareous cement, columnar | Hard |
| Coal | 0.90 | 71.38 | | Lumpy, mainly containing dark coal | |
| Siltstone | 19.17 | 90.55 | | Mud or calcareous cement, relatively broken | |
| Packsand | 2.28 | 92.83 | | Containing feldspar, quartz, calcareous cement | |
| Coal | 0.80 | 93.63 | | Lumpy, mainly containing dark coal | |
| Siltstone | 14.06 | 107.69 | | Cross-bedding, argillaceous cement, columnar, $f$ = 7.5 | Main roof Hard |
| Carbon mudstone | 0.50 | 108.19 | | Black, lumpy, containing plant fossils | |
| Siltstone | 4.90 | 113.09 | | The core is broken, argillaceous cemented | Immediate roof |
| Coal | 8.60 | 122.20 | | Columnar, weak glass luster, jagged fracture, $f$ = 3.8 | No.5 coal Hard |
| Packsand | 7.99 | 130.19 | | Containing feldspar, quartz, calcareous cement | |
| Glutenite | 1.50 | 131.69 | | Mainly metamorphic and sedimentary rocks | |
| Medium sandstone | 17.70 | 149.39 | | Containing feldspar, quartz, calcareous cement | |

**Figure 2.** Borehole diagram of the Yushuling Coal Mine.

The 110501 working face mainly has the following safety problems: ① The Yushuling Coal Mine is a new mine after expansion, and there are no relevant measured data; ② the No. 5 coal seam and the main roof are hard, so to strengthen the top coal caving effect, the shearer cutting height was designed to be 4 m, so the coal rock pressure of the large mining height top coal caving face may be very large and impactive; ③ the working face was buried at a depth of 100 to 150 m, the rock is full bedrock, and the changes in rock pressure and WFFZ should be different from those in typical shallow coal seams with a TRBT less than 1.

### *2.2. Aquifer Condition*

There are four groups of aquifers in this mine, namely quaternary loose rock pore phreatic aquifer ($H_1$), Jurassic Ahe Formation aquifer ($H_2$), burnt rock aquifer ($H_3$), and Jurassic Talicq Formation aquifer ($H_4$), among which the burnt rock aquifer is rich in water. The burnt rock is a rock formation baked by a spontaneous combustion coal seam. The burnt rock has extremely developed fissure, good connectivity, and strong water content, thus forming a better water storage space, namely burnt rock aquifer. There is a large area of burnt rock aquifer in Yushuling Coal mine, and it is estimated by transient electromagnetic exploration that the static reserves of groundwater in the burning area are about 452,000 $m^3$. The hydrogeological map of the mine is shown in Figure 3.

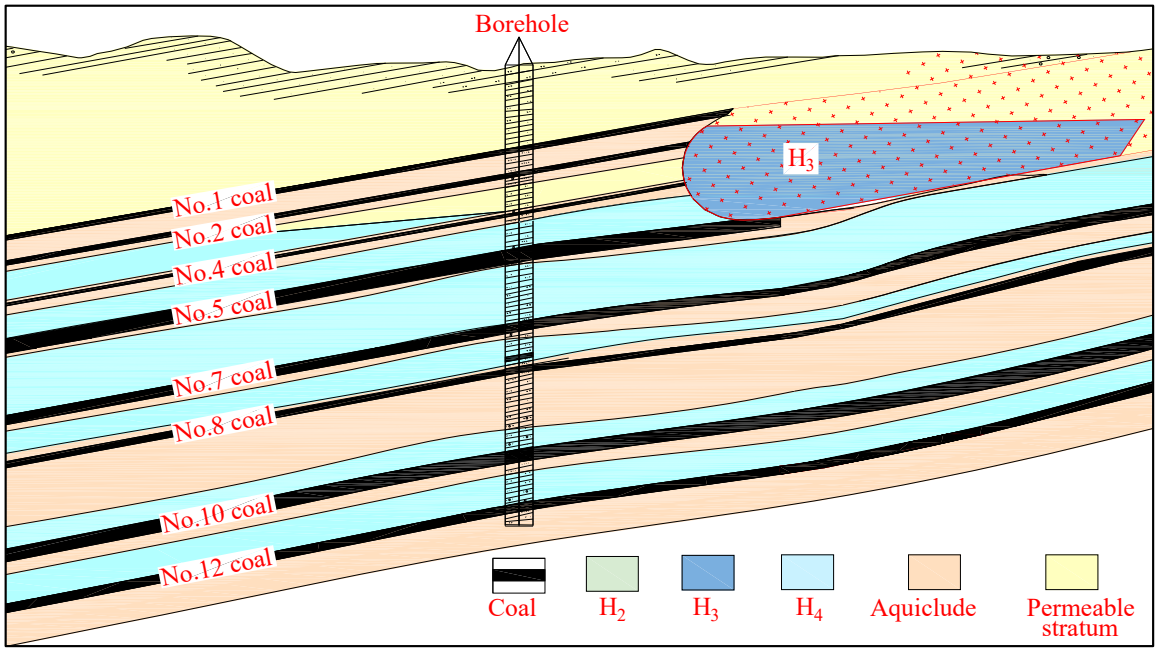


**Figure 3.** The hydrogeological map of Yushuling Coal Mine.

As shown in Figure 4, the surface bedrock of Yushuling Coal Mine is bare, vegetation is sparse and gullies are developed, in some areas, the fractures are grid-shaped, with 6~8 fractures per square meter, and sometimes dozens of fractures, with the width of 2~5 mm. Rainwater and melted snow collect in the gullies and leak down the fissures to recharge the groundwater, which form deep water storage structures in some areas and connect with the burnt rock aquifer. Mining leads to an increase in overburden fissures and the formation of the WFFZ. When the WFFZ is connected with the aquifer in the burning area or to the surface water, the water inflow increases suddenly, which easily causes water inrush accidents. In addition, the cracks leading to the surface also aggravate the problem of spontaneous combustion in the goaf. Therefore, it is very important to study the development law of the WFFZ.

(**a**) (**b**)

**Figure 4.** Mine surface topography. (**a**) Surface gullies. (**b**) Surface fractures.

## 3. Mine Pressure and Roadway Deformation

### *3.1. Simulation Scheme*

To study the evolution of abutment pressure, the stress and deformation of the mining roadway during the mining process of SHCSHRFB, FLAC$^{3D}$ 6.0 numerical software was used to simulate the advance of the 110501 working face; the constitutive model is the Mohr–Coulomb model. The mining simulation of the 110501 working face can be divided into the stage before the extended open-off cut, the stage between the extended open-off cut and the abandoned open-off cut, and the stage after the abandoned open-off cut. The above three stages correspond to the advance lengths of 0 to 65 m, 65 m to 160 m, and 160 to 370 m, respectively. The numerical model is shown in Figure 5; the strata parameters are shown in Table 1.

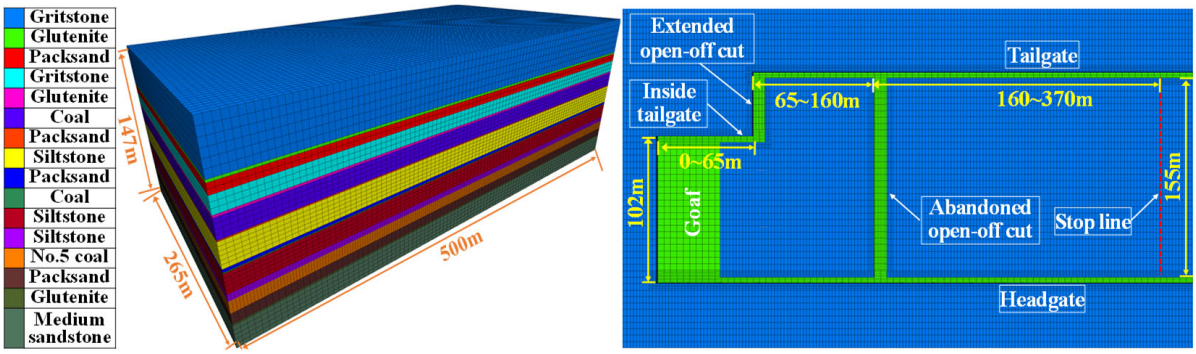


**Figure 5.** Numerical model of the 110501 working face.

**Table 1.** Strata parameters of numerical model.

| SN | Lithology | Thickness (m) | Density (kg/m$^3$) | Bulk Modulus (MPa) | Shear Modulus (MPa) | Tension Strength (MPa) | Friction Angle (°) |
|---|---|---|---|---|---|---|---|
| 1 | Gritstone | 34.08 | 2490 | 2679 | 1764 | 1.49 | 43.15 |
| 2 | Glutenite | 1.80 | 2540 | 2886 | 1901 | 1.72 | 39.6 |
| 3 | Packsand | 7.40 | 2630 | 2643 | 1820 | 1.46 | 40.23 |
| 4 | Gritstone | 11.68 | 2490 | 2679 | 1764 | 1.49 | 43.15 |
| 5 | Glutenite | 1.70 | 2540 | 2886 | 1901 | 1.72 | 39.6 |
| 6 | Coal | 0.60 | 1350 | 2139 | 1204 | 0.78 | 48.23 |
| 7 | Packsand | 13.8 | 2630 | 2643 | 1820 | 1.46 | 40.23 |

**Table 1.** *Cont.*

| SN | Lithology | Thickness (m) | Density (kg/m$^3$) | Bulk Modulus (MPa) | Shear Modulus (MPa) | Tension Strength (MPa) | Friction Angle (°) |
|---|---|---|---|---|---|---|---|
| 8 | Siltstone | 19.17 | 2660 | 3550 | 2345 | 1.38 | 39.6 |
| 9 | Packsand | 2.28 | 2630 | 2643 | 1820 | 1.46 | 40.23 |
| 10 | Coal | 0.80 | 1350 | 2139 | 1204 | 0.78 | 48.23 |
| 11 | Siltstone | 14.06 | 2660 | 3550 | 2345 | 1.38 | 39.6 |
| 12 | Siltstone | 5 | 2660 | 3550 | 2345 | 1.38 | 39.6 |
| 13 | No. 5 coal | 8.6 | 1350 | 2139 | 1204 | 0.78 | 48.23 |
| 14 | Packsand | 7.99 | 2630 | 2643 | 1820 | 1.46 | 40.23 |
| 15 | Glutenite | 1.50 | 2540 | 2886 | 1901 | 1.72 | 39.6 |
| 16 | Medium sandstone | 17.70 | 2630 | 2643 | 1820 | 1.46 | 40.23 |

### 3.2. Abutment Pressure

The abutment pressure distribution during of the advance of the 110501 working face is shown in Figure 6 and Table 2: during the advance of the working face to 370 m, the front and side abutment pressure increased continuously, but when the advance length of the working face was greater than the length of the working face, for example, beyond 155 m, the change in the peak value of the abutment pressure and its position from the working face was not obvious. When the working face advanced to 370 m, the peak front and side abutment pressures were 3.9 MPa and 4.1 MPa, respectively, which were found at 10 m and 11 m ahead of the working face, and the front influence ranges of abutment pressures were 19 m and 21 m, respectively. Considering that the in situ stress on the 110501 working face was 2.2 MPa, the peak abutment pressure concentration factor was less than 2, implying that the stress concentration was weak.

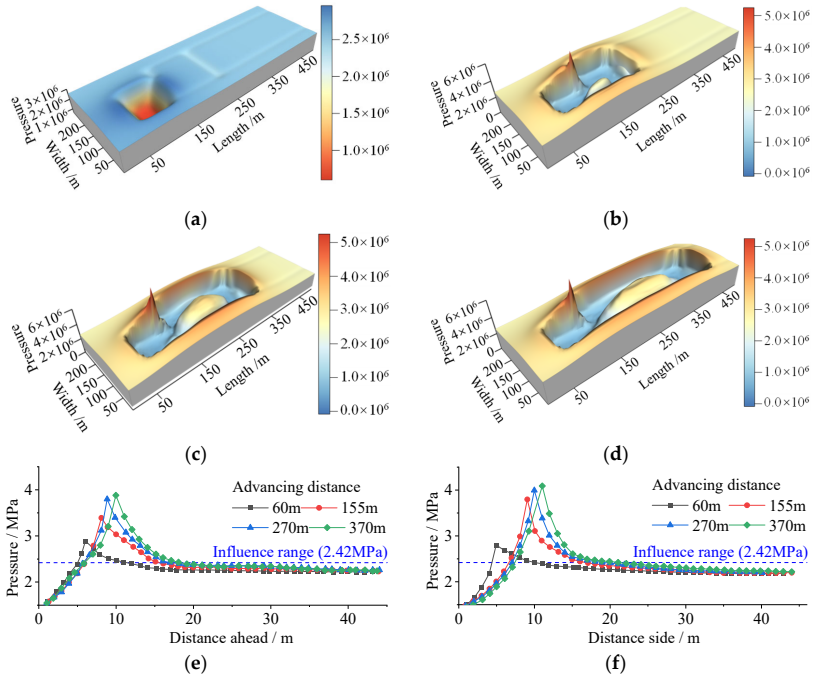


**Figure 6.** Abutment pressure variation as the working face advances. (**a**) Advance of 60 m. (**b**) Advance of 155 m. (**c**) Advance of 270 m. (**d**) Advance of 370 m. (**e**) Front abutment pressure. (**f**) Side abutment pressure.

**Table 2.** Abutment pressure parameters.

| Abutment Pressure | Advance Distance | 60 m | 155 m | 270 m | 370 m |
|---|---|---|---|---|---|
| Front abutment pressure | Peak stress | 2.9 | 3.4 | 3.8 | 3.9 |
| | Peak stress distance from working face | 6 | 8 | 9 | 10 |
| | Influence distance | 12 | 16 | 18 | 19 |
| Side abutment pressure | Peak stress | 2.8 | 3.8 | 4.0 | 4.1 |
| | Peak stress distance from working face | 5 | 9 | 10 | 11 |
| | Influence distance | 10 | 16 | 19 | 21 |

Before the 110501 working face advanced to 65 m, the working face length was 102 m, and the side abutment pressure was less than the front abutment pressure, but when the 110501 working face advanced from between 155 m and 370 m, the length of the working face reached 155 m, and at this time the side abutment pressure exceeded the front abutment pressure. This is because the advance length of the working face in the early stage of mining is less than the length of the working face, and so the peak abutment pressure on the side with the larger span is usually greater. The vertical stress on the coal at the junction of the extended open-off cut and the inside tailgate was larger, reaching a maximum of 6.8 MPa. Therefore, the support of this area should be strengthened to prevent large deformation.

### *3.3. The Deformation and Stress of the Extended Open-Off Cut*

The initial length of the open-off cut in the 110501 working face is 102 m. After the 110501 working face advanced to the extended open-off cut, the length of the working face increased to 155 m. The roof subsidence and the vertical stress of surrounding rock at different positions of the extended open-off cut are shown in Figure 7: the closer to the inside tailgate, the larger the roof subsidence and the vertical stress of the extended open-off cut, and the range that was significantly affected by the mining of the working face was within 15 m of the extended open-off cut. When the working face was 25 m and 45 m from the extended open-off cut, the roof subsidence and the maximum vertical stress of the surrounding rock were not affected by mining at the face; when the working face was 5 m from the extended open-off cut, the roof subsidence of the extended open-off cut near the inside tailgate was increased rapidly to 66 mm, and the maximum vertical stress increased from 2.94 MPa to 3.77 MPa; therefore, when the working face is less than 25 m from the extended open-off cut, the support of the extended open-off cut within 15 m from the inside tailgate should be strengthened.

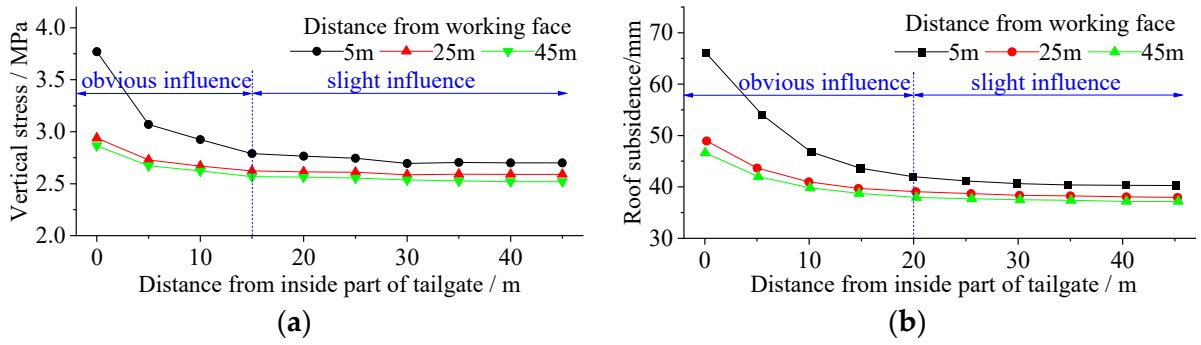


**Figure 7.** Vertical stress and roof subsidence of extended open-off cut. (**a**) Vertical stress. (**b**) Roof subsidence.

### *3.4. The Deformation and Stress of the Maingate*

Figure 8 illustrates the vertical stress of surrounding rock and roof subsidence of the maingate at up to 40 m in front of the working face when working face 110501 advanced to 370 m: with the increasing distance from the working face, the vertical stress and surrounding rock deformation of the maingate were continuously reduced. The obvious influence distances of the stress and surrounding rock deformation were within 20 m and 15 m in front of the working face, respectively. At 40 m in front of the working face, the maximum vertical stress of the maingate reduced from 3.8 MPa to 2.68 MPa, and the maximum roof subsidence of the maingate reduced from 46 mm to 27.4 mm. On the whole, the deformation and stress concentration of the maingate were small, and the range of influence of the maingate by the mining of the 110501 working face was about 20 m, so it is appropriate to set the front roadway support distance to 20 m.

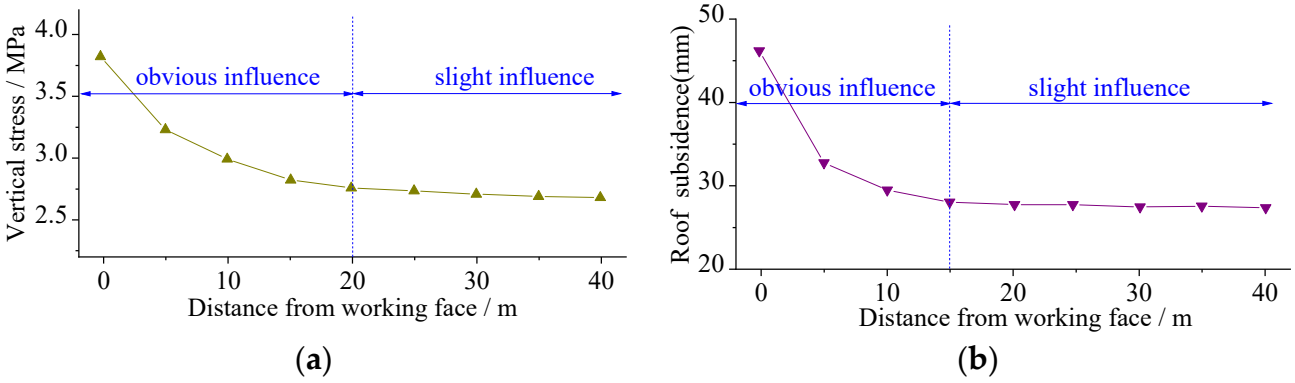


**Figure 8.** Vertical stress and roof subsidence of maingate. (**a**) Vertical stress. (**b**) Roof subsidence.

## 4. Roof Breaking and WFFZ Development

### *4.1. Physical Similarity Simulation Scheme*

#### 4.1.1. Model Parameters

To assess the breaking and movement characteristics of the overburden, the height of the WFFZ and the abutment pressure in SHCSHRFB, a physical similarity simulation model for mining at the 110501 working face was designed. The model frame measures 2.5 m × 0.3 m × 1.5 m, and the designed geometric similarity ratio was 100:1. The two sides of the model and the bottom plate were fixed, and 0.2 m coal pillars on both sides of the model were reserved to eliminate border effects, making the simulated working face advance length 210 m. Similar materials were made by mixing different proportions of gypsum, calcium carbonate, sand, and water. The total height of the model is 1317 mm, and there are 18 layers of strata, including all rock layers from the floor to the surface of the 110501 working face. The basic parameters and proportions of similar materials of the physical similarity model are shown in Tables 3 and 4.

**Table 3.** The basic parameters of the physical similarity model.

| Parameter | Value | Parameter | Value |
|---|---|---|---|
| Model length | 2.5 m | Geometric ratio | 100:1 |
| Model width | 0.3 m | Stress ratio | 167:1 |
| Model height | 1317 mm | Movement ratio | 10:1 |
| Coal seam thickness | 86 mm | Density ratio | 1.667:1 |
| Mining height | 40 mm | Mining step distance | 3.2 m |
| Top coal height | 46 mm | Mining step interval | 30 min |

#### 4.1.2. Mining and Monitoring of the Model

The simulated mining method is as follows: mining the bottom coal with one step distance and then mining the top coal with the previous step distance. The thicknesses of

the bottom coal and top coal excavated are 40 mm and 46 mm, respectively. Each mining step distance is 32 mm, and the cycle is carried out successively until the mining distance reaches 210 mm.

**Table 4.** The proportions of similar materials of the physical similarity model.

| SN | Lithology | Sand (kg) | Calcium Carbonate (kg) | Gypsum (kg) | Thickness (cm) | Cumulative Thickness (cm) |
|---|---|---|---|---|---|---|
| 1 | Gritstone | 252.00 | 25.20 | 10.80 | 32.00 | 131.70 |
| 2 | Packsand | 53.28 | 4.00 | 9.32 | 7.40 | 99.70 |
| 3 | Gritstone | 91.35 | 9.14 | 3.92 | 11.60 | 92.30 |
| 4 | Glutenite | 20.25 | 3.38 | 3.38 | 3.00 | 80.70 |
| 5 | Packsand | 102.24 | 7.67 | 17.89 | 14.20 | 77.70 |
| 6 | Siltstone | 129.60 | 21.60 | 21.60 | 19.20 | 63.50 |
| 7 | Packsand | 21.60 | 1.62 | 3.78 | 3.00 | 44.30 |
| 8 | Siltstone | 94.50 | 15.75 | 15.75 | 14.00 | 41.30 |
| 9 | Siltstone | 42.00 | 2.52 | 5.88 | 5.60 | 27.30 |
| 10 | No. 5 coal | 64.50 | 3.87 | 9.03 | 8.60 | 21.70 |
| 11 | Packsand | 57.60 | 4.32 | 10.08 | 8.00 | 13.10 |
| 12 | Glutenite | 24.30 | 4.05 | 4.05 | 3.60 | 5.10 |
| 13 | Medium sandstone | 11.57 | 0.58 | 1.35 | 1.50 | 1.50 |

The model monitoring instrument and layout are shown in Figure 9. The BZ2205C stress sensors, which were placed in the coal seam 50 m, 100 m, and 150 m away from the open-off cut, were used to record the abutment pressure of the working face. The non-contact full-field strain measurement system (MatchID-2D v.2019) was used to monitor the displacement of the strata, which includes the analysis software, camera, lighting and notebook. The software uses the method of digital image capture and recognition to analyse the deformation of the physical model. Firstly, the model surface needs to be whitewashed and black spots are spotted. Then, the software performs binarisation and image analysis on the photos taken, and finally, the displacement cloud map in the process of model excavation is obtained.

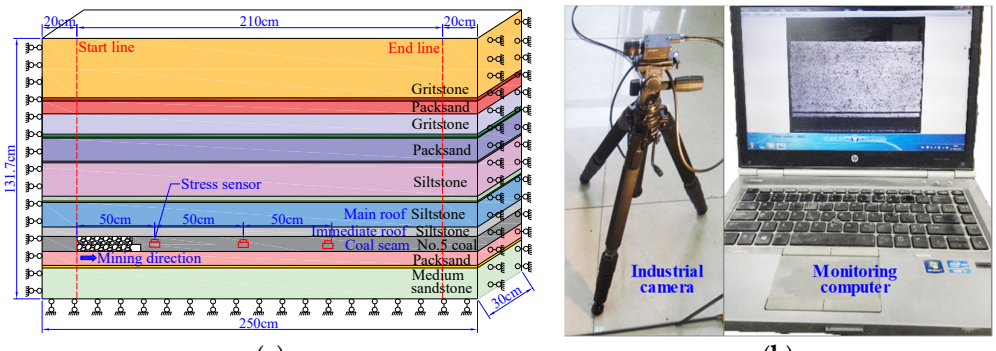


(**a**) (**b**)

**Figure 9.** Model layout and monitoring equipment. (**a**) Physical similarity model. (**b**) Monitoring equipment.

### *4.2. Roof Breaking Characteristics*

The roof breaking characteristics of the 110501 working face under different equivalent advance distances are shown in Figure 10: the first and second breaking distances of the immediate roof were 12.8 m and 9.6 m, respectively. The main roof collapsed for the first time when the working face advanced to 38.4 m; due to the large first collapse distance, the problem of strong rock pressure may occur, so some preventive measures should be taken in the mining process.

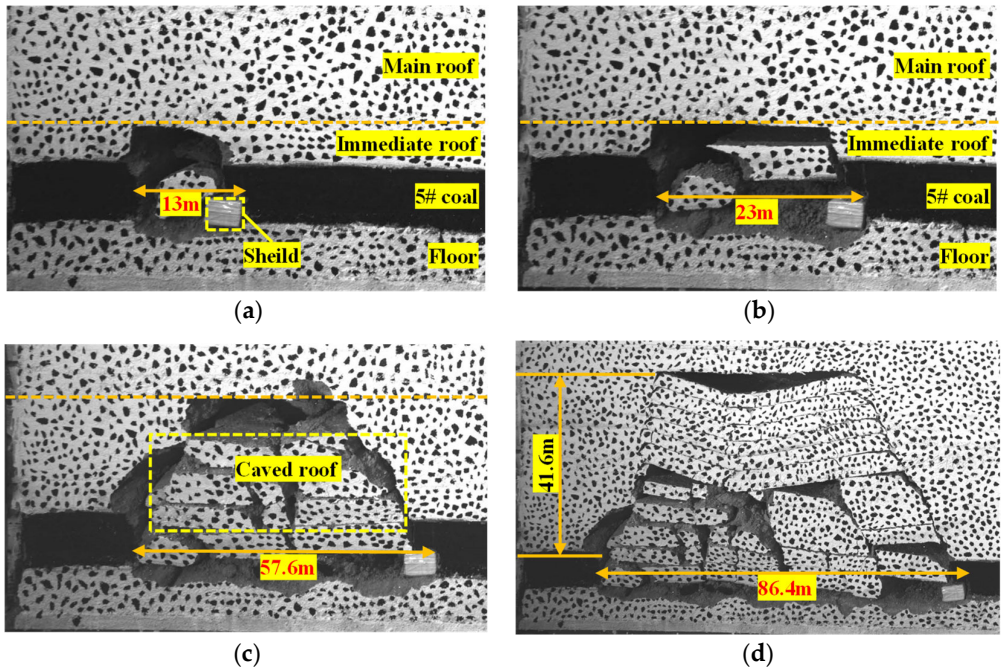


**Figure 10.** Main roof breaking characteristics of the 110501 working face. (**a**) Advance of 13 m. (**b**) Advance of 23 m. (**c**) Advance of 57.6 m. (**d**) Advance of 86.4 m.

When the main roof collapsed for the third time, the strata about 20 m above the main roof collapsed simultaneously, and the height of WFFZ developed to 41.6 m. As the 110501 working face advanced to 210 m, the main roof collapsed eight times, and the corresponding advance distances were 38.4 m, 62.4 m, 86.4 m, 112.0 m, 134.4 m, 160.0 m, 185.6 m, and 208 m, respectively; the average collapse distance was 26 m. Overall, the collapse distance of the main roof is not very large and should not cause strong rock pressure problems.

### *4.3. Development of the WFFZ*

The development of the WFFZ in the 110501 working face can be divided into three main stages: initial development, rapid development, and stability, corresponding to the advance lengths of 0 m to 86.4 m, 86.4 m to 112 m, and 112 m to 210 m, respectively.

Figure 11 shows that when the working face advanced to 38.4 m, horizontal cracks developed directly above the top of the immediate roof and the height of the crack was 12.8 m above the No. 5 coal seam. When the working face advanced to 59.2 m, horizontal cracks were formed above the main roof, and their height reached 31.2 m. At this stage, no vertical cracks were generated in the overlying strata, and the horizontal cracks did not penetrate each other. At that time, the water conductivity of the cracks was poor.

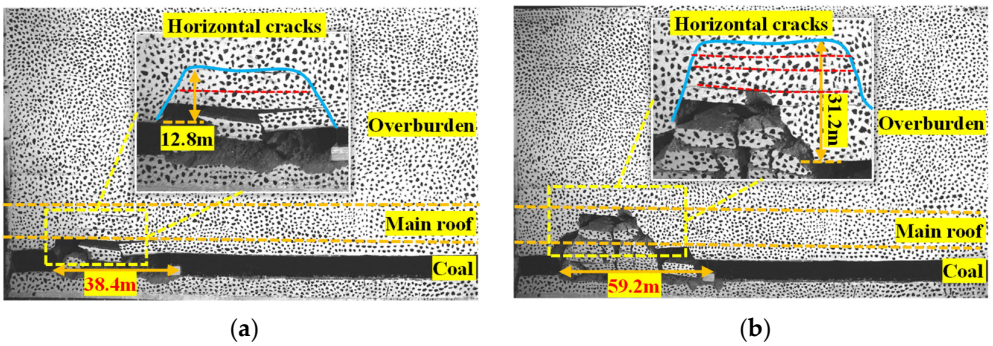


**Figure 11.** Initial stage of WFFZ formation. (**a**) Advance of 38.4 m. (**b**) Advance of 59.2 m.

Figure 12 shows that when the working face advanced to 86.4 m, the WFFZ height rapidly rose to 53.6 m. Some cracks within the height range of 41.6 m to 53.6 m were only horizontal cracks with a small opening size, which were not connected to the lower cracks. At 41.6 m above the coal seam, a 3 m to 4 m gap was created between the siltstone and the upper 13.2 m thick, hard, fine sandstone. When the working face advanced to 112 m, the WFFZ developed rapidly to 83 m, and at this time, the gap at 41.6 m above the coal seam reclosed.

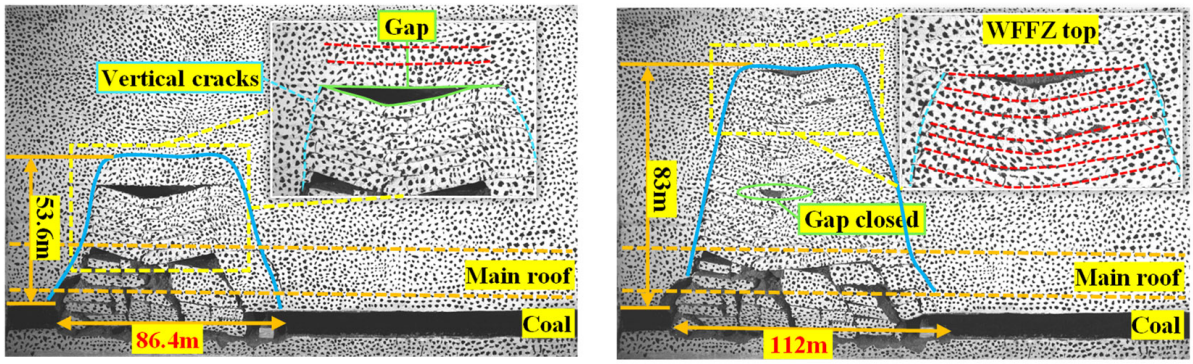


(**a**) (**b**)

**Figure 12.** Rapid development of the WFFZ. (**a**) Advance of 86.4 m. (**b**) Advance of 112 m.

Figure 13 shows that compared with conditions when the working face advanced to 112 m, the height of the WFFZ does not increase further when the working face advanced to 208 m, and the opening width and length of the horizontal cracks in the WFFZ were smaller than those of the vertical cracks. Four large sub-vertical fractures, each with a height of about 80 m, were formed when the working face advanced to 112.0 m, 121.6 m, 160.0 m, and 208 m. The 34 m thick rock layer on the surface above the 110501 working face was not broken, forming a continuous bending zone.

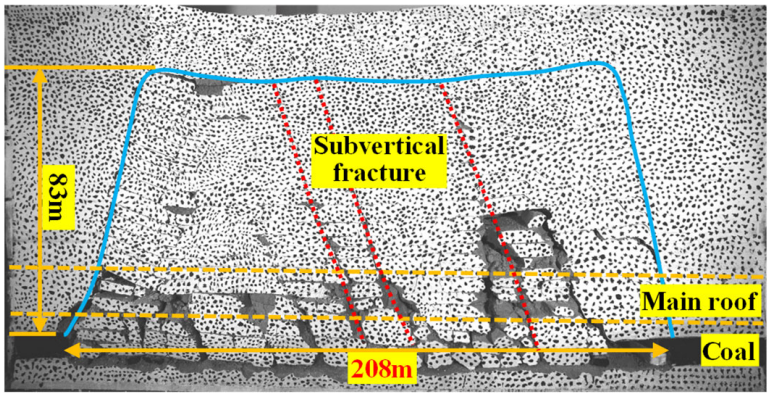


**Figure 13.** Stabilisation of the WFFZ.

### *4.4. Front Abutment Pressure*

Figure 14 shows the vertical stress monitored by a stress sensor placed at 150 m from the open-off cut; when the stress sensor was 20 m from the working face, the monitored vertical stress was maintained at about 2.2 MPa. When the distance from the working surface reduced to 7 m, the vertical stress gradually increased to a peak value of 3.3 MPa; therefore, at the 110501 working face, the front abutment pressure raised some 7 m from the working face, and the range of influence of the front abutment pressure was about 20 m to 25 m, which is closer to that predicted by numerical simulation.

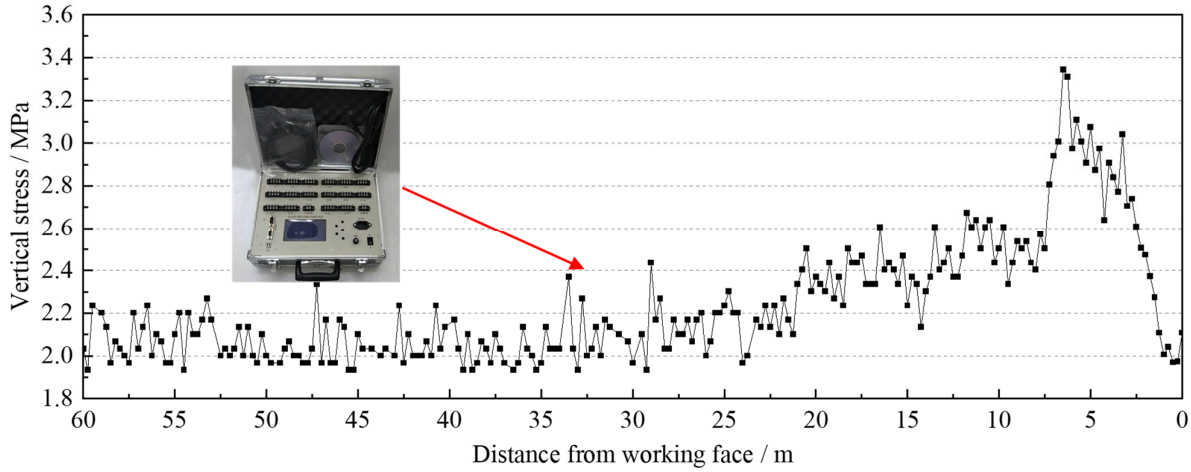


**Figure 14.** Front abutment pressure monitored using stress sensor.

## 5. Engineering Practice

### *5.1. Working Face Weighting and Support Effect*

In consideration of the large first collapse distance obtained from the physical simulation, the roof pre-splitting blasting was carried out in the open-off cut to prevent the possible strong rock pressure. The hydraulic support column pressure and support effect of the 110501 working face are shown in Figure 15: under the support afforded by ZF10000/23/45 hydraulic supports (Henan Heavy Industry, Kaifeng, China), the working face undergoes no rib falling, and there is no hydraulic support overload during mining. The first weighting distance is 33.5 m, the average periodic weighting distance is 26.9 m, and the dynamic load coefficient is between 1.08 and 1.16. The intensity of the weighting is very weak, and there is no strong rock pressure that usually appears in typical shallow coal seams (Table 5).

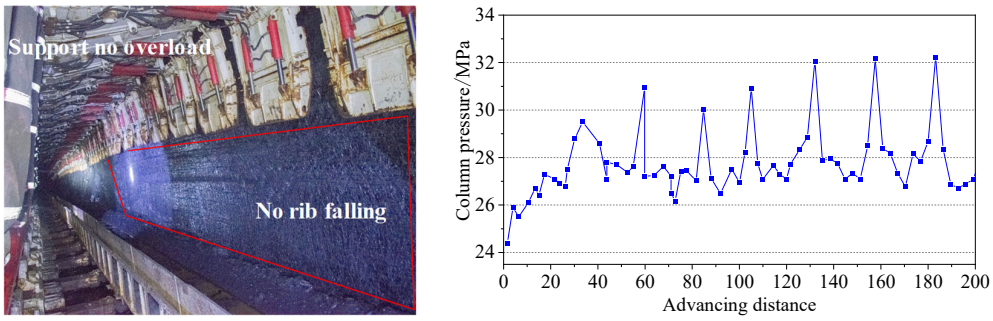


(**a**) (**b**)

**Figure 15.** Column pressure and working face support result. (**a**) Working face support result. (**b**) hydraulic support column pressure.

**Table 5.** Weighting characteristics of the 110501 working face.

| Weighting Times | 1 | 2 | 3 | 4 | 5 | 6 | 7 | Mean |
|---|---|---|---|---|---|---|---|---|
| Pressure/MPa | 29.5 | 30.9 | 30.0 | 31.5 | 32.0 | 32.2 | 32.2 | 30.8 |
| Dynamic factor | 1.08 | 1.13 | 1.13 | 1.10 | 1.15 | 1.16 | 1.16 | 1.11 |
| Weighting distance/m | 33.5 | 26.3 | 25 | 26 | 27 | 25.6 | 25.6 | 25.8 |

### *5.2. Deformation of Maingate and Extended Open-Off Cut*

The section of the 110501 maingate is rectangular, with a width of 5000 mm and a height of 3300 mm. A bolt-net-cable support system was adopted, the row and column

spacing of bolts in roof and ribs was 800 mm × 800 mm, and the row and column spacing of cables in the roof was 2000 mm × 3000 mm. As shown in Figure 16, roof separation and deformation could be seen when the working face was about 30 m from the measuring station, and the speed of separation and roadway deformation increased at about 15 m from the working face. The maximum roof subsidence, roof strata separation, and deformation of the left- and right-hand ribs of the roadway were 17.7 mm, 13.8 mm, 7.6 mm, and 4.9 mm, respectively, making it appropriate to set the front maingate support distance to 15 to 20 m.

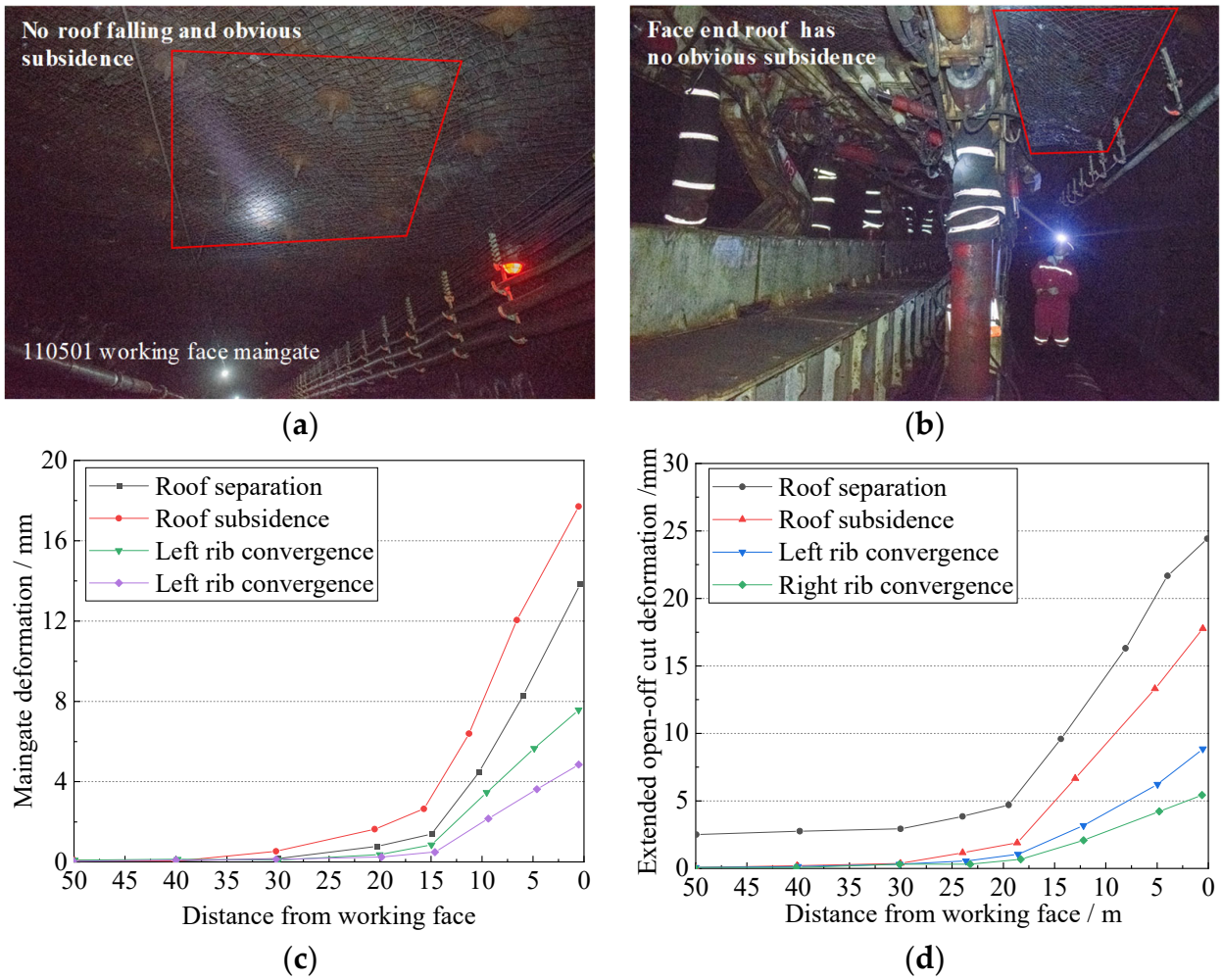


**Figure 16.** Support effect in maingate and extended open-off cut. (**a**) Maingate roof deformation photo. (**b**) Face end deformation photo. (**c**) Maingate deformation value. (**d**) Extended open-off cut deformation value.

The 110501 extended open-off cut has a rectangular section with a width of 9500 mm and a height of 3300 mm. A bolt-net-cable support system was adopted, and the row and column spacing of bolts and roof cables in roof and ribs were 800 mm × 800 mm and 2250 mm × 3000 mm, respectively. It can be seen from Figure 15 that due to the larger section size of the 110501 extended open-off cut, roof subsidence of 2.5 mm occurred during the driving stage. The separation and surrounding deformation began to increase at about 30 m from the measuring station, and the speed of separation and roadway deformation increased at about 18 m from the working face. The maximum roof subsidence, roof separation, and displacement of the left- and right-hand sides of the roadway were 24.4 mm, 17.8 mm, 8.9 mm, and 5.4 mm, respectively. To ensure safety, the extended open-off cut was closed when the 110501 working face was 30 m away and workers were not permitted to enter that space, the deformation was monitored through the in situ monitoring system.

In general, the deformation of surrounding rock in the maingate and extended open-off cut of the 110501 working face is very small, and the roadways are stable and meet the requirements for safe mining.

### *5.3. Field Detection of WFFZ*

#### 5.3.1. Detection Scheme

It can be seen from Figure 17 that, the height of the WFFZ was detected using a water-injection method. We drilled a hole diagonally above the working face, then used a double-capsule sealer to conduct section-by-section water injection and finally determined the fracture zone height from the changes in water injection flow rate. Initially, using the common empirical formula used in China to calculate the height of the hydraulic fracture zone, when the overlying rock is a medium-hard rock layer, the empirical formula for the WFFZ is as follows:

$$H_{Li} = \frac{100\sum M}{1.6\sum M + 3.6} + 5.6 \text{ or } H_{Li} = 20\sqrt{\sum M} + 10 \quad (1)$$

where $H_{Li}$ is the height of the WFFZ and $\sum M$ is the cumulative mining thickness. The height of the WFFZ calculated using the two formulae represent 55.1 m and 68.7 m, respectively, and the WFFZ height obtained from physical similarity modelling is 83 m. To ensure clear observation, the end of the observation borehole was designed to be 90 m above the working surface. Figure 18 shows the layout of both control and observation boreholes: the boreholes were drilled from the roof of the 110503 tailgate to the overburden of the 110501 working face.

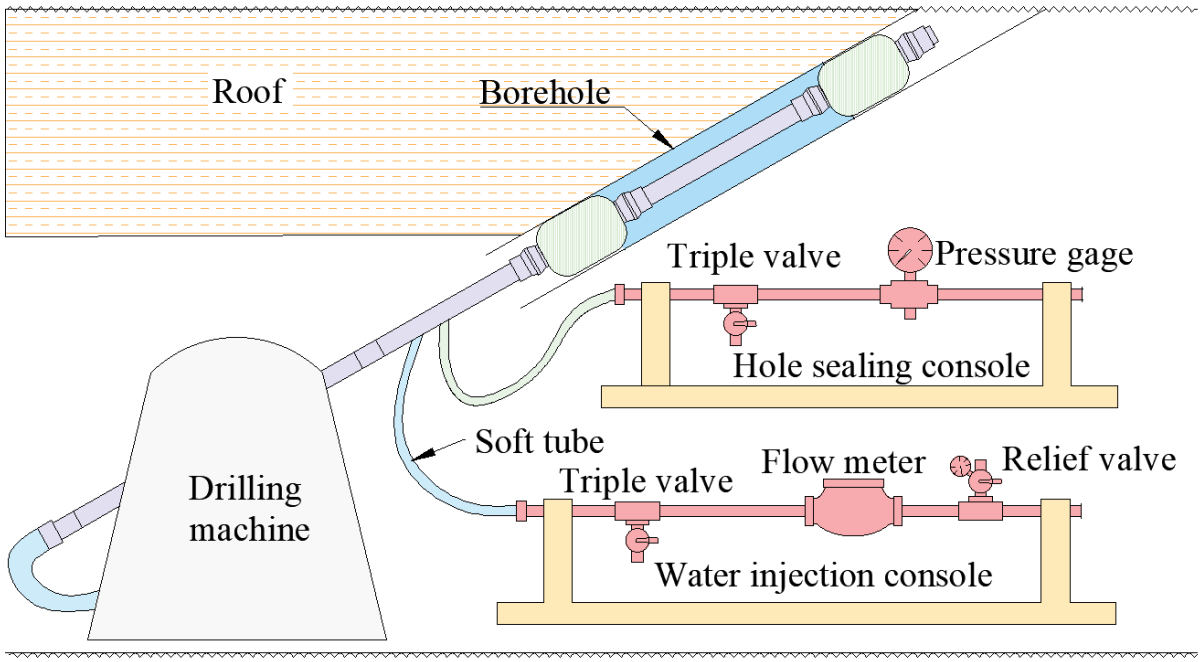


**Figure 17.** Schematic diagram of the water-injection method using double-capsule sealer.

As the main roof of the 110501 working face is relatively hard, its roof movement stabilizes after about 2 months or more. The 110501 working face advanced by 3.2 to 4 m per day, so the observation borehole distance from the 110501 working face should be no less than 200 m. To improve the accuracy of WFFZ detection, a control borehole S1 and three observation boreholes S2 to S4 were drilled. The borehole parameters are shown in Table 6.

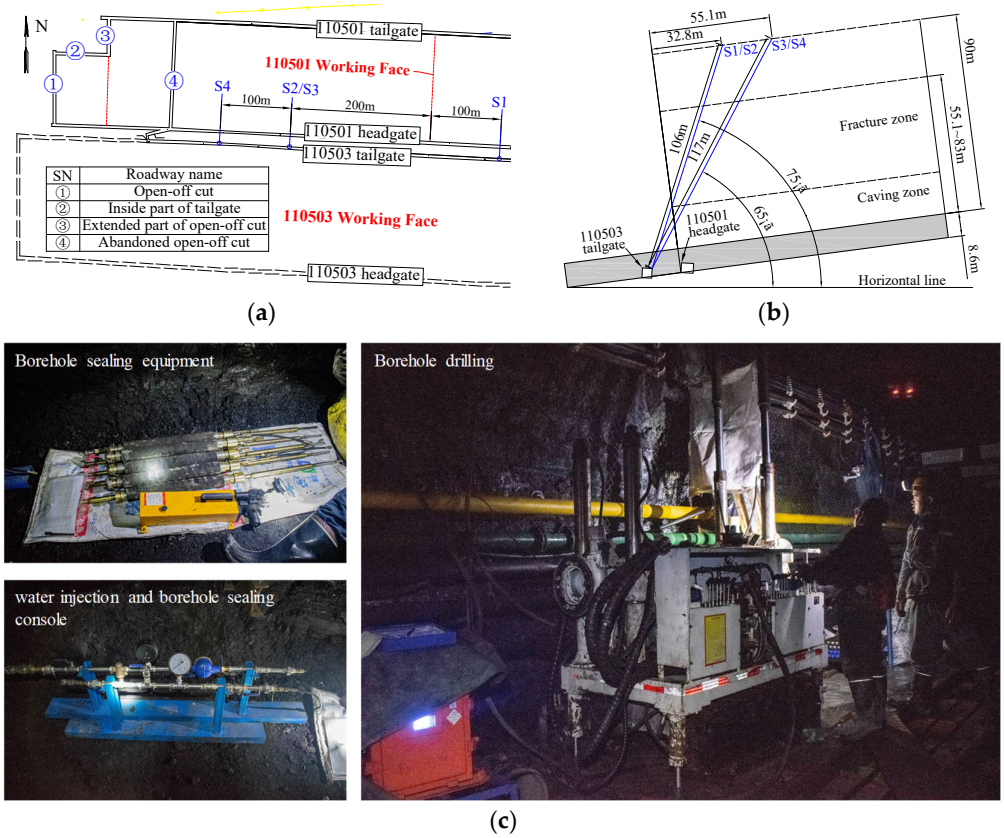


**Figure 18.** Borehole layout and equipment of WFFZ observation. (**a**) Top view of observation borehole. (**b**) Section view of observation borehole. (**c**) Observation equipment.

**Table 6.** Observation borehole parameters.

| Borehole Name | Diameter | Angle | Length | Height | Distance from 110501 Face | Type |
|---|---|---|---|---|---|---|
| S1 | 75 mm | 75° | 117 m | 90 m | 100 m ahead | Control borehole |
| S2 | 75 mm | 75° | 117 m | 90 m | 200 m behind | Observation borehole |
| S3 | 75 mm | 65° | 117 m | 90 m | 200 m behind | Observation borehole |
| S4 | 75 mm | 65° | 117 m | 90 m | 300 m behind | Observation borehole |

#### 5.3.2. WFFZ Observations

It can be seen from Figure 19 that borehole S2 with an elevation angle of 75° has a small flow change within the first 90 m, indicating that it may not pass through the WFFZ due to inappropriate elevation or drilling errors. Within the range of 70 m to 85 m above the working face, the flows in boreholes S3 and S4 both increased significantly, returning average flows of 0.73 L/min and 0.95 L/min, respectively; the water flow in boreholes S3 and S4 decreased rapidly from 85 m and 87 m, respectively. Between 70 m and 90 m above the working surface, the flow in the control hole S1 was between 0.25 L/min and 0.4 L/min, so the maximum development height of the WFFZ is 87 m; however, considering that the observation borehole is long, there will be some offset in the drilling direction, and the borehole end is located near the middle of the working face, rather than the highest position of the WFFZ near the boundary of the working face. So, the actual maximum height of the water-conducting fracture zone may be greater than 90 m. In summary, the field measured height of the WFFZ is closer to the 83 m obtained by physical similar simulation, but it is quite different from the empirical formula, which proves that the empirical formula is not accurate when used to predict the WFFZ in SHCSHRFB.

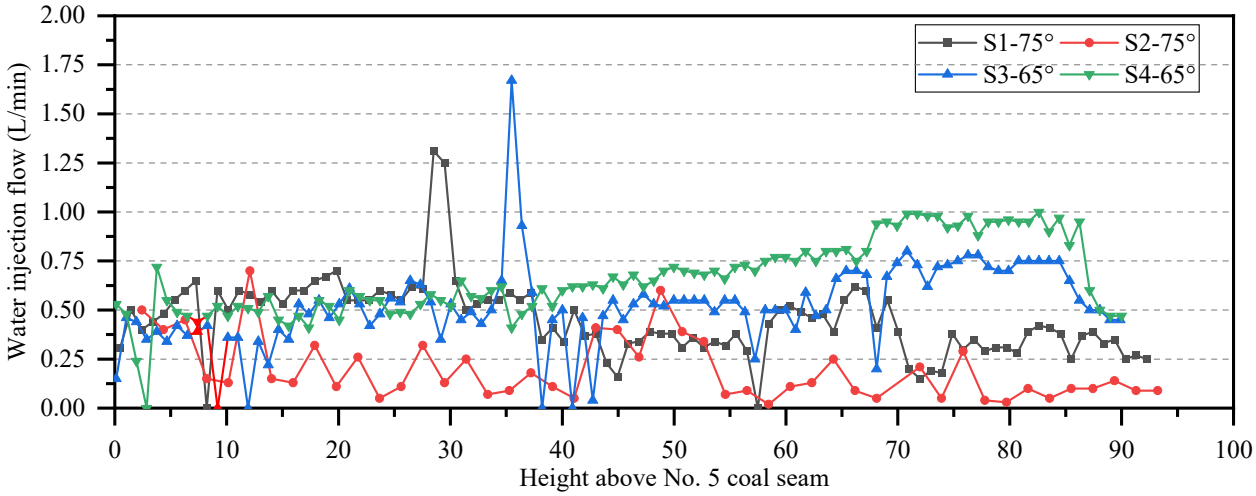


**Figure 19.** Observations from boreholes in the WFFZ.

## 6. Conclusions

Based on the engineering conditions of the 110501 working face in Yushuling Coal Mine, the abutment pressure of the working face, surrounding rock stress, and deformation of the roadways were analysed, the breaking of the immediate roof and the main roof during advancing were studied, and the development of the WFFZ was analysed and measured in situ. The main conclusions are as follows:

1. The numerical simulation results show that the influence distance of abutment pressure and the abutment pressure peak and its position relative to the working face continue to increase as the working face advances. After the advance distance exceeds the length of the working face (155 m), the abutment pressure tends to stabilize; when the working face advances to 370 m, the front and side abutment pressure peaks are 3.9 MPa and 4.1 MPa, respectively, and are located at 10 m and 11 m in front of the working face: the corresponding zones of influence ahead of the working face reach 19 m and 21 m, respectively. The abutment pressure peak concentration factor is less than 2, which shows that the mining pressure intensity is weak. The extended open-off cut and maingate within 20 m in front of the working face are affected by mining and should be reinforced prior to mining.
2. The physical similarity simulation shows that the first collapse distance of the 110501 working face is 32 m and the average collapse distance is 26 m; the development of the WFFZ can be divided into the initial development stage (advancing over the first 86.4 m), rapid development stage (advancing from 86.4 to 112 m), and the stable stage (advancing beyond 112 m); the maximum heights of the WFFZ in these three stages are 31.2 m, 53.6 m, and 83 m, respectively.
3. The average weighting interval of the 110501 top coal caving face (as measured in-situ) is 26.9 m, which is similar to the collapse distance obtained from physical similarity modelling; the maximum dynamic load factor during the weighting period is 1.16. The deformation of the extended open-off cut and maingate is mainly within 20 m in front of the working face; the maximum development height of the WFFZ is 87 m according to in situ monitoring, which is close to the physical similar simulation results, but quite different from those arising from use of the empirical formula. The rock pressure in SHCSHRFB is relatively weak, which is significantly different from that of typical shallow-buried thin bedrock working faces.

**Author Contributions:** Conceptualisation, Z.W. and Q.S.; methodology, Z.W. and Q.S.; software, Z.W.; validation, Y.W.; formal analysis, Z.W.; investigation, Y.W.; resources, Q.S.; data curation, Z.W.; writing—original draft preparation, Z.W.; writing—review and editing, Z.W. and Q.S.; visualisation, Z.W. and Y.W.; supervision, Q.S.; funding acquisition, Z.W and Q.S. All authors have read and agreed to the published version of the manuscript.

**Funding:** This work was supported by the Postgraduate Research and Practice Innovation Program of Jiangsu Province [grant number KYCX21_2371] and the "Scientists + Engineers" Team for Water Conservation Mining of Extra-Thick Coal Seam [grant number 2024QCY-KXJ-055].

**Institutional Review Board Statement:** Not applicable.

**Informed Consent Statement:** Not applicable.

**Data Availability Statement:** The data used to support the findings of this study are included within the article.

**Acknowledgments:** The authors would like to thank Chengfang Shan and other technicians of Kuqa Yushuling Coal Mine for providing the engineering data, equipment, and conditions needed for this study.

**Conflicts of Interest:** The authors declare no conflicts of interest.

## References

1. Xue, J.; Shi, L.; Wang, H.; Ji, Z.; Shang, H.; Xu, F.; Zhao, C.; Huang, H.; Luo, A. Water abundance evaluation of a burnt rock aquifer using the AHP and entropy weight method: A case study in the Yongxin coal mine, China. *Environ. Earth Sci.* **2021**, *80*, 417. [CrossRef]
2. Qin, D.D.; Wang, X.F.; Zhang, D.S.; Guan, W.M.; Zhang, L.; Xu, M.T. Occurrence Characteristic and Mining Technology of Ultra-thick Coal Seam in Xinjiang, China. *Sustainability* **2019**, *11*, 6470. [CrossRef]
3. Li, J.M.; Huang, Y.L.; Zhang, J.X.; Li, M.; Qiao, M.; Wang, F.W. The Influences of Key Strata Compound Breakage on the Overlying Strata Movement and Strata Pressure Behavior in Fully Mechanized Caving Mining of Shallow and Extremely Thick Seams: A Case Study. *Adv. Civ. Eng.* **2019**, *2019*, 5929635. [CrossRef]
4. Huang, Q.X.; He, Y.P. Research on Overburden Movement Characteristics of Large Mining Height Working Face in Shallow Buried Thin Bedrock. *Energies* **2019**, *12*, 4208. [CrossRef]
5. Wang, S.R.; Wu, X.G.; Zhao, Y.H.; Hagan, P. Mechanical Performances of Pressure Arch in Thick Bedrock during Shallow Coal Mining. *Geofluids* **2018**, *2018*, 2419659. [CrossRef]
6. Liu, Y.J.; Qi, Q.J.; Wang, A.H. Influence of Valleys Terrain on Pressure of Fully Mechanized Working Faces in Shallow Coal Seams. *Shock Vib.* **2021**, *2021*, 8880041. [CrossRef]
7. Wang, J.; Ning, J.G.; Tan, Y.L.; Hu, S.C.; Guo, W.Y. Deformation and failure laws of roadway surrounding rock and support optimization during shallow-buried multi-seam mining. *Geomat. Nat. Hazards Risk* **2020**, *11*, 191–211. [CrossRef]
8. Zhao, J.; Liu, C.; Li, J. Stress field distribution and strata behavior characteristics in shallow thick coal seam mining in gully region. *Caikuang Yu Anquan Gongcheng Xuebao/J. Min. Saf. Eng.* **2018**, *35*, 742–750. [CrossRef]
9. Mondal, D.; Roy, P.N.S.; Kumar, M. Monitoring the strata behavior in the Destressed Zone of a shallow Indian longwall panel with hard sandstone cover using Mine-Microseismicity and Borehole Televiewer data. *Eng. Geol.* **2020**, *271*, 105593. [CrossRef]
10. Xu, Z.H.; Li, Q.S.; Li, X.B. Overburden Migration and Failure Characteristics in Mining Shallow Buried Coal Seam with Thick Loose Layer. *Adv. Mater. Sci. Eng.* **2020**, *2020*, 9024751. [CrossRef]
11. Huang, Q.X.; He, Y.P.; Cao, J. Experimental Investigation on Crack Development Characteristics in Shallow Coal Seam Mining in China. *Energies* **2019**, *12*, 1302. [CrossRef]
12. Gao, R.; Huo, B.J.; Xia, H.C.; Meng, X.B. Numerical simulation on fracturing behaviour of hard roofs at different levels during extra-thick coal seam mining. *R. Soc. Open Sci.* **2020**, *7*, 191383. [CrossRef] [PubMed]
13. Lan, Y.W.; Gao, R.; Yu, B.; Meng, X.B. In Situ Studies on the Characteristics of Strata Structures and Behaviors in Mining of a Thick Coal Seam with Hard Roofs. *Energies* **2018**, *11*, 2470. [CrossRef]
14. Gu, S.T.; Jiang, B.Y.; Pan, Y.; Liu, Z. Bending Moment Characteristics of Hard Roof before First Breaking of Roof Beam Considering Coal Seam Hardening. *Shock Vib.* **2018**, *2018*, 7082951. [CrossRef]
15. Sun, Q.; Shan, C.; Wu, Z.; Wang, Y. Case Study: Mechanism and Effect Analysis of Presplitting Blasting in Shallow Extra-Thick Coal Seam. *Arch. Min. Sci.* **2022**, *67*, 381–399. [CrossRef]
16. Yan, H.; Zhang, J.X.; Li, B.Y.; Zhu, C.L. Crack propagation patterns and factors controlling complex crack network formation in coal bodies during tri-axial supercritical carbon dioxide fracturing. *Fuel* **2021**, *286*, 119381. [CrossRef]
17. Huang, B.X.; Liu, J.W.; Zhang, Q. The reasonable breaking location of overhanging hard roof for directional hydraulic fracturing to control strong strata behaviors of gob-side entry. *Int. J. Rock Mech. Min. Sci.* **2018**, *103*, 1–11. [CrossRef]
18. Yardimci, A.G.; Karakus, M. A new protective destressing technique in underground hard coal mining. *Int. J. Rock Mech. Min. Sci.* **2020**, *130*, 104327. [CrossRef]

19. Gesualdo, A.; Minutolo, V.; Nunziante, L. Failure in Mohr-Coulomb soil cavities. *Can. Geotech. J.* **2001**, *38*, 1314–1320. [CrossRef]
20. Gesualdo, A.; Minutolo, V.; Nunziante, L. Local collapse in soft rock bank cavities. *J. Geotech. Geoenviron. Eng.* **2001**, *127*, 1037–1042. [CrossRef]
21. Huang, Q.; Du, J.; Hou, E.; Yang, F. Research on overburden and ground surface cracks distribution and formation mechanism in shallow coal seams group mining. *Caikuang Yu Anquan Gongcheng Xuebao/J. Min. Saf. Eng.* **2019**, *36*, 7–15. [CrossRef]
22. Zhang, K.; Yang, T.H.; Bai, H.B.; Gamage, R.P. Longwall Mining-Induced Damage and Fractures: Field Measurements and Simulation Using FDM and DEM Coupled Method. *Int. J. Geomech.* **2018**, *18*, 04017127. [CrossRef]
23. Van Dyke, M.A.; Zhang, P.; Dougherty, H.; Su, D.; Kim, B.H. Identifying Longwall-Induced Fracture Zone Height Through Core Drilling. *Min. Metall. Explor.* **2022**, *39*, 1345–1355. [CrossRef]
24. Liu, Y.; Yuan, S.C.; Yang, B.B.; Liu, J.W.; Ye, Z.Y. Predicting the height of the water-conducting fractured zone using multiple regression analysis and GIS. *Environ. Earth Sci.* **2019**, *78*, 422. [CrossRef]
25. Du, W.; Chai, J.; Zhang, D.; Lei, W. The study of water-resistant key strata stability detected by optic fiber sensing in shallow-buried coal seam. *Int. J. Rock Mech. Min. Sci.* **2021**, *141*, 104604. [CrossRef]
26. Hebblewhite, B. Fracturing, caving propagation and influence of mining on groundwater above longwall panels-a review of predictive models. *Int. J. Min. Sci. Technol.* **2020**, *30*, 49–54. [CrossRef]
27. Xu, Y.J.; Ma, L.Q.; Yu, Y.H. Water Preservation and Conservation above Coal Mines Using an Innovative Approach: A Case Study. *Energies* **2020**, *13*, 2818. [CrossRef]
28. Sun, Q.; Zhang, J.X.; Zhou, N.; Qi, W.Y. Roadway Backfill Coal Mining to Preserve Surface Water in Western China. *Mine Water Environ.* **2018**, *37*, 366–375. [CrossRef]
29. Fan, G.W.; Zhang, D.S.; Zhang, S.Z.; Zhang, C.G. Assessment and Prevention of Water and Sand Inrush Associated with Coal Mining Under a Water-filled Buried Gully: A Case Study. *Mine Water Environ.* **2018**, *37*, 565–576. [CrossRef]